Editors' Suggestion

Operator Scaling Dimensions and Multifractality at Measurement-Induced Transitions

A. Zabalo,[1] M. J. Gullans,[2,3] J. H. Wilson,[1,4,5] R. Vasseur,[6] A. W. W. Ludwig,[7] S. Gopalakrishnan,[8,9] David A. Huse,[2] and J. H. Pixley[1,2,10]

[1]*Department of Physics and Astronomy, Center for Materials Theory, Rutgers University, Piscataway, New Jersey 08854, USA*
[2]*Department of Physics, Princeton University, Princeton, New Jersey 08544, USA*
[3]*Joint Center for Quantum Information and Computer Science, NIST/University of Maryland, College Park, Maryland 20742, USA*
[4]*Department of Physics and Astronomy, Louisiana State University, Baton Rouge, Louisiana 70803, USA*
[5]*Center for Computation and Technology, Louisiana State University, Baton Rouge, Louisiana 70803, USA*
[6]*Department of Physics, University of Massachusetts, Amherst, Massachusetts 01003, USA*
[7]*Department of Physics, University of California, Santa Barbara, California 93106, USA*
[8]*Department of Physics, The Pennsylvania State University, University Park, Pennsylvania 16802, USA*
[9]*Department of Physics and Astronomy, CUNY College of Staten Island, Staten Island, New York 10314, USA*
[10]*Center for Computational Quantum Physics, Flatiron Institute, 162 5th Avenue, New York, New York 10010, USA*

(Received 30 July 2021; accepted 5 January 2022; published 3 February 2022)

Repeated local measurements of quantum many-body systems can induce a phase transition in their entanglement structure. These measurement-induced phase transitions (MIPTs) have been studied for various types of dynamics, yet most cases yield quantitatively similar critical exponents, making it unclear how many distinct universality classes are present. Here, we probe the properties of the conformal field theories governing these MIPTs using a numerical transfer-matrix method, which allows us to extract the effective central charge, as well as the first few low-lying scaling dimensions of operators at these critical points for $(1+1)$-dimensional systems. Our results provide convincing evidence that the generic and Clifford MIPTs for qubits lie in different universality classes and that both are distinct from the percolation transition for qudits in the limit of large on-site Hilbert space dimension. For the generic case, we find strong evidence of multifractal scaling of correlation functions at the critical point, reflected in a continuous spectrum of scaling dimensions.

DOI: 10.1103/PhysRevLett.128.050602

The dynamics of an open quantum system can be viewed as unitary evolution interspersed with events where an environment *measures* the system. This competition between entangling dynamics and collapsing measurements leads to a measurement-induced phase transition (MIPT) between phases with distinct entanglement structure [1–13]. By increasing the frequency of measurements, the system goes from a volume-law phase where the entanglement entropy of a subsystem scales with its volume to an area-law phase where it scales with its boundary. This transition occurs in the individual "trajectories" but is invisible in the mixed state averaged over measurement outcomes.

MIPTs exist in various classes of dynamics [14–27], have been observed experimentally [28], and are analytically tractable in certain limits, interpreted as a percolation transition [1,8,9]. Even away from tractable limits, the numerically extracted critical exponents of the MIPT are close to the values for percolation [7]. These observations raise the question: Are MIPTs resulting from different dynamics in distinct universality classes?

Beyond classifying the universal nature of MIPTs, developing precise characterizations of this class of critical phenomena has motivations in quantum information and computational complexity theory. In particular, an entanglement transition potentially signifies a phase transition in the resources required to represent the quantum state on a classical computer [29,30]. Such quantum information-theoretic observables lack natural counterparts in the conventional framework of statistical physics. Consequently, our understanding of the "relevant" degrees of freedom in describing the related critical phenomena remains nascent.

This work presents evidence that MIPTs in different classes of random circuits belong to distinct universality classes beyond percolation. These conclusions are supported by a numerical exploration of the nonunitary conformal field theories (CFTs) with central charge $c = 0$ governing the MIPTs for three classes of dynamics—generic (Haar), dual-unitary, and Clifford random circuits, each with random single-site measurements of Pauli operators. The emergence of conformal invariance at MIPTs is suggested by mappings onto statistical models [8,9,31] and confirmed in previous

numerical work [11]. We probe the properties of these CFTs by numerically computing several leading Lyapunov exponents of the transfer matrix. The Lyapunov exponents are related to the scaling dimensions characterizing the scaling of *typical* [32] observables of the CFT, the first of which is related to the "effective central charge" c_{eff} [33]—a universal number [34] distinguishing CFTs with central charge $c = 0$.

We find evidence that the MIPT for generic circuits belongs to a different universality class than that for Clifford circuits, while both differ from percolation. The effective central charge is distinct in the two cases: $c_{\text{eff}}^{H} \approx 0.25(3)$ and $c_{\text{eff}}^{C} \approx 0.37(1)$, respectively. We compare these numerical values to the predictions of large on-site Hilbert space ($d \to \infty$) mappings onto percolation: $c_{\text{eff}}^{H,d\to\infty} \approx 0.291$ for Haar and $c_{\text{eff}}^{C,d=2^n\to\infty} \approx 0.365$ for Clifford qudit circuits. Dual-unitary circuits have a transition in the generic universality class, but their symmetries allow us to extract the effective central charge $c_{\text{eff}}^{\text{DU}} = 0.24(2)$ and the leading Lyapunov exponents with higher precision. We also find evidence that the spectra of operators at MIPTs are distinct from those in the percolation CFT. Thus the generic and Clifford MIPTs appear to be governed by two distinct CFTs and differ from any previously known instances. Last, we demonstrate multifractality in the generic MIPT in a chain of qubits.

From quantum channels to CFTs.—Consider a quantum circuit with a fixed set of unitary gates and measurement locations and times. The hybrid unitary or measurement dynamics is described through the quantum channel

$$\mathcal{N}_t(\rho) = \sum_{\mathbf{m}} K_{\mathbf{m}} \rho K_{\mathbf{m}}^{\dagger}, \tag{1}$$

where ρ is the system's density matrix, and $K_{\mathbf{m}} = K_t^{m_t} K_{t-1}^{m_{t-1}} \ldots K_1^{m_1}$ is a Kraus operator. The operators $K_s^{m_s} = P_s^{m_s} U_s$ consist of random unitary gates U_s and random projectors $P_s^{m_s}$ onto measurement outcomes m_s. Each summand $K_{\mathbf{m}} \rho K_{\mathbf{m}}^{\dagger}$ in Eq. (1) represents a "quantum trajectory" of the system. Moreover, $\text{Tr}(K_{\mathbf{m}} \rho K_{\mathbf{m}}^{\dagger}) = p_{\mathbf{m}}(\rho)$ is the probability of the set of outcomes $\mathbf{m}$. We suppress the argument ρ since at late times the probabilities $p_{\mathbf{m}}$ become independent of the initial density matrix at the critical point.

Following Ref. [11], we posit that each trajectory can be identified with a $(1+1)$-dimensional statistical mechanics model, defined implicitly through the identification that its partition function $Z_{\mathbf{m}} \equiv p_{\mathbf{m}}$. Without defining an explicit model, we note that the partition functions of canonical statistical mechanics models can be written as tensor networks with a similar structure to the single-trajectory circuit [35], so this identification is natural. The trajectories making up a particular channel form an ensemble of statistical mechanics models with quenched spacetime randomness due to the measurement outcomes. Each model's weight in the ensemble is set by its Born probability $p_{\mathbf{m}}$.

It follows from these observations that, for a circuit of fixed length L, a layer of time evolution for a particular trajectory [i.e., the map $\rho \to \mathcal{T}_t \rho \mathcal{T}_t^{\dagger}$, where $\mathcal{T}_j = K_{2j}^{m_{2j}} K_{2j-1}^{m_{2j-1}}$ is depicted in Fig. 1(a)] acts as a transfer matrix for the statistical mechanics model describing that trajectory. Note that one can write $Z_{\mathbf{m}} = \sum_i (\sigma_i^{\mathbf{m}})^2$, where $(\sigma_i^{\mathbf{m}})^2$ are the eigenvalues of $K_{\mathbf{m}} K_{\mathbf{m}}^{\dagger}$, i.e., the squares of the singular values of $K_{\mathbf{m}}$. Equivalently, these are the eigenvalues of an initially completely mixed density matrix that is purified by the evolution [5]. At late times, $K_{\mathbf{m}}$ is given by a large product of the operators $\mathcal{T}_j$ and $\sigma_i^{\mathbf{m}}$ decays exponentially, as the state purifies. This exponential decay motivates the definition of trajectory dependent exponents [32,36] $\lambda_i^{\mathbf{m}}$, through $[\sigma_i^{\mathbf{m}}(t)]^2 = e^{\lambda_i^{\mathbf{m}} t}$ as $t \to \infty$; note that

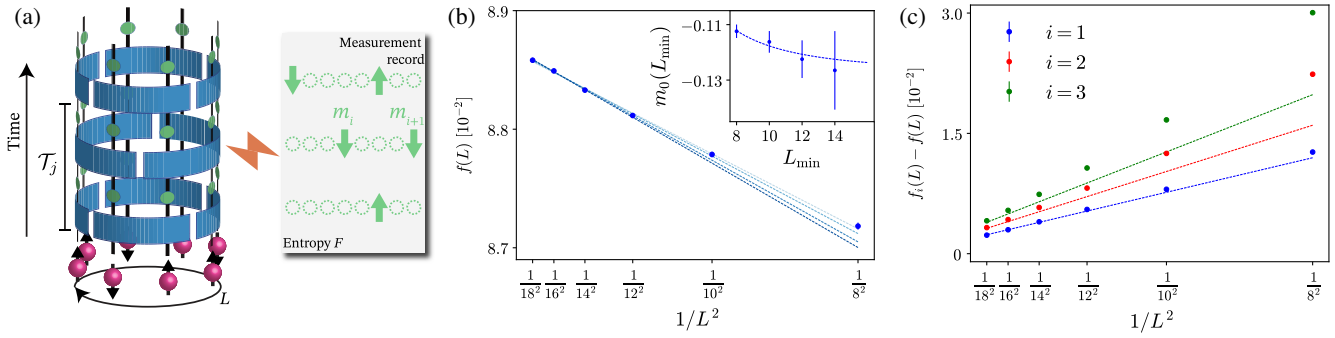

FIG. 1. (a) The cylindrical geometry of the random circuit model for a system of qubits of length L with periodic boundary conditions. The blue rectangles represent the entangling gates and the green dots are the location of measurements. The time evolution can be viewed as a product of transfer matrices denoted by $\mathcal{T}_j$ whose leading Lyapunov exponent is given by the entropy of the measurement record F. (b) The free energy density displays the $1/L^2$ dependence expected from Eq. (3), allowing us to extract c_{eff}. Darker blue indicates increasing $L_{\min} = 8 \to 14$. (Inset) To improve our estimate we successively remove the smallest system size from the fit and find $m_0(L_{\min})$ which contains the leading order correction to Eq. (3). The dotted line corresponds to the fit $m_0(L) = -0.13 + (0.98/L^2)$. (c) The differences of the generalized free energy densities, $f_i(L) - f(L)$, show the $1/L^2$ behavior expected from Eq. (4). The dotted lines correspond to the extrapolated values $m_i(L_{\min} \to \infty)$. The data shown is for the dual unitary model at $p = p_c \approx 0.14$ and 25000 samples for $L = 8$, 10, 12, 14, 16 and 10000 for $L = 18$.

$\lambda_i^{\mathbf{m}} < 0$, and we compute them as specified in Ref. [37]. We then average $\lambda_i^{\mathbf{m}}$ over trajectories (using the Born weights $p_{\mathbf{m}}$) to yield the Lyapunov exponents $\lambda_0, \lambda_1, \lambda_2, \ldots$ in descending order.

The leading Lyapunov exponent of the transfer matrix has an appealing interpretation. In general, this quantity is the free energy of the statistical mechanics model up to a factor of time, i.e., $t\lambda_0^{\mathbf{m}} = \ln p_{\mathbf{m}}$. Averaging the free energy with Born weights gives us that $F/t = -\lambda_0$, where

$$F = -\sum_{\mathbf{m}} p_{\mathbf{m}} \ln p_{\mathbf{m}}. \tag{2}$$

This averaged free energy is the Shannon entropy of the measurement record, see Fig. 1(a).

As in more conventional disordered systems, the averaged free energy can be computed within a replica formalism. Introducing the annealed average replicated partition function $\bar{Z}_r = \sum_{\mathbf{m}} p_{\mathbf{m}} Z_{\mathbf{m}}^r$, where r is the replica index, the corresponding annealed average free energy is $F_r = -\ln \bar{Z}_r$. The quenched average free energy from Eq. (2) is then given by $F = \lim_{r\to 0}(dF_r/dr)$ in the replica limit $r \to 0$. The annealed average replicated statistical model has a phase transition for finite $r > 0$, which we assume is described by a CFT whose properties approach those of the MIPT in the $r \to 0$ limit.

Effective central charge and operator spectrum.—The central charge $c(r)$ of the CFT describing the replicated model $\bar{Z}_r$ goes to $c(r) \to 0$ in the replica limit $r \to 0$; this follows from the trivial partition function $\bar{Z}_{r\to 0} = 1$. However, standard CFT results on a cylinder of circumference L and length t (in the limit $t \gg L$) imply that the averaged free energy density $F(L,t)/A = f(L)$ [33,36] scales as

$$f(L) = f(L=\infty) - \frac{\pi c_{\text{eff}}}{6L^2} + \ldots, \tag{3}$$

where $c_{\text{eff}} = \lim_{r\to 0}(dc(r)/dr)$ is a universal number called the effective central charge, and $A \equiv \alpha L t$ is the effective spacetime area. Since the statistical mechanics model is only defined implicitly, its intrinsic space and time scales (and the anisotropy α between them) must be extracted numerically, as we discuss below.

We now turn to the subleading Lyapunov exponents. In the statistical mechanics picture, the difference of the two leading Lyapunov exponents controls the decay of correlations along the direction of the transfer matrix, i.e., it determines the scale on which initial conditions are forgotten. The next-to-leading Lyapunov exponent thus corresponds to the most relevant (i.e., longest-lived) operator while higher Lyapunov exponents correspond to faster-decaying operators. Conformal invariance dictates how these quantities behave at critical points:

$$f_i(L) - f(L) = 2\pi x_i^{\text{typ}}/L^2, \tag{4}$$

where $f_i(L) = -\lambda_i/(\alpha L)$ is obtained from the Lyapunov exponents ($i = 1, 2, \ldots$) and x_i^{typ} is the scaling dimension of the ith most relevant operator characterizing the decay of *typical* [32] correlators, defined only in the generic case—averaged correlators will be discussed below.

Circuit models.—We consider two main ensembles of random circuits: Haar random circuits with two-qubit gates chosen from the Haar measure and stabilizer circuits with gates chosen from the Clifford group. Stabilizer circuits have an efficient classical algorithm for the simulation of the single-circuit observables studied in this work [38]. Additionally, we consider subclasses of Haar and Clifford circuits in which all gates are "dual unitary" [39,40], i.e., unitary in both space and time directions. The most generic dual unitary gates are given by $U = e^{i\phi}(u_+ \otimes u_-) \cdot V[J] \cdot (v_- \otimes v_+)$, where $\phi, J \in \mathbb{R}$, $u_\pm, v_\pm \in \mathrm{SU}(2)$, and $V[J] = \exp\{-i(\pi/4)\sigma^x \otimes \sigma^x + (\pi/4)\sigma^y \otimes \sigma^y + J\sigma^z \otimes \sigma^z]\}$ [39]. We present evidence that the dual unitary Haar (Clifford) circuits lie within the same universality class as Haar (Clifford) circuits (to within our numerical precision, see below). However, these circuits allow for a more accurate estimate of the critical properties since their statistical self-duality under spacetime rotations forces $\alpha = 1$ and the associated rescaling factors are known exactly [37]. Below, all results are taken at the critical point determined using the ancilla order parameter described in Ref. [10]. We find $p_c^H = 0.17(1)$, $p_c^{\text{DU}} = 0.14(1)$, $p_c^C = 0.1596(3)$, and $p_c^{\text{DC}} = 0.205(1)$ for the Haar, dual unitary, Clifford, and dual Clifford models, respectively [7,37].

The anisotropy parameters for the Haar and Clifford models are estimated by comparing the correlation functions along the space and time directions. These correlation functions are determined in the quantum circuit by computing the mutual information between two ancilla qubits separated in space and time [7,10]. In the Haar model, $\alpha^H = 0.81(9)$ while for the stabilizer model $\alpha^C = 0.62(3)$. As a check, we compute the anisotropy for the dual unitary variants and find $\alpha^{\text{DU}} = 1.0(1)$ in agreement with the known value $\alpha = 1$ [37].

Numerical approach.—We now discuss our algorithm for finding the leading Lyapunov exponents in the Haar and dual unitary models (see Ref. [37] for the approach used for Clifford and percolation models). The first few singular values $\sigma_i^{\mathbf{m}}(t)$ are computed by picking a random initial state, generating a set of mutually orthogonal vectors to the initial state, and iteratively applying the same set of transfer matrices $\mathcal{T}_j$ [depicted in Fig. 1(a)] to the set. Each projector in $\mathcal{T}_j$ is chosen based on the Born probability of the time-evolved initial state and after each application of $\mathcal{T}_j$ the set is re-orthogonalized. This allows us to estimate F in Eq. (2) and $f_i(L) = -\lambda_i/(\alpha L)$ in Eq. (4) [37] through a Monte Carlo sampling of the Born probabilities [37]. We note that our results are sensitive to the initial state at early times; to achieve results independent of initial conditions, we wait for an "equilibration" time of $\tau = 4L$ and average

over different initial states (see Supplemental Material [37]). This approach agrees well with a direct evaluation of the spectrum of the transfer matrix on small system sizes [37].

Results.—The data for the leading Lyapunov exponent at long times provide an estimate of $F(t \to \infty)$ and are shown in Fig. 1(b). We find that this displays a clear linear behavior as a function of $1/L^2$ with slope m_0 related to the effective central charge as expected from Eq. (3). To improve our estimate of m_0, we can successively remove smaller system sizes, $L < L_{\min}$, from the fit and write $m_0(L_{\min}) = m_0(\infty) + (b/L_{\min}^2)$, which accounts for the leading order correction to Eq. (3). The procedure is illustrated in Fig. 1(b) and its inset. Using $c_{\text{eff}} = -(6m_0(\infty)/\pi)$, we find $c_{\text{eff}}^H = 0.25(3)$ for the Haar model with an improved estimate of $c_{\text{eff}}^{\text{DU}} = 0.24(2)$ from the dual unitary variant. Similarly, $c_{\text{eff}}^C = 0.37(1)$ for the stabilizer circuit [37]. A rudimentary analysis of c_{eff} as a function of p displays a broad maximum near p_c suggesting deviations within the uncertainty of p_c should not significantly affect the quoted values (results not shown). These values can be compared to the exact predictions for large on-site Hilbert space dimension $d \to \infty$, where the MIPT maps onto percolation. Following methods developed in prior work [8,9,31,41,42], we find $c_{\text{eff}}^{H,d\to\infty} = [5\sqrt{3}(1-\gamma)/4\pi] = 0.291\ldots$ in the Haar case and, using additional properties of the Clifford group proved in Ref. [43], $c_{\text{eff}}^{C,d=2^n\to\infty} = 0.365\ldots$ for stabilizer circuits [37]. Our numerical estimate of c_{eff}^C for qubits ($d = 2$) is consistent with the percolation value ($d = 2^n \to \infty$), thus more exponents (or universal data) are needed to distinguish those two universality classes.

The differences between Lyapunov exponents, $f_i(L) - f(L) \sim 1/L^2$, as expected [Fig. 1(c)]; the slope of the fitted line, $m_i(L_{\min})$ can then be used to determine x_i^{typ}. The scaling dimension x_1^{typ} is related to the (typical) bulk exponent of the "order parameter, "$x_1^{\text{typ}} = \eta/2$ [10]. Our estimates for the Haar model $\eta^H/2 = 0.14 \pm 0.02$ and the dual unitary variant $\eta^{\text{DU}}/2 = 0.122 \pm 0.001$ are consistent with the result $\eta/2 \approx 0.125$ for the mutual information computed in Ref. [7], for Renyi indices $n > 1$, and are close to, but outside of error bars from, the percolation value $\eta/2 = (5/48) \approx 0.104$. The next lowest scaling dimensions are given by $x_2^{\text{typ}} = 0.18(2)$ and $x_3^{\text{typ}} = 0.23(3)$ for the Haar model and $x_2^{\text{typ}} = 0.163(1)$ and $x_3^{\text{typ}} = 0.202(1)$ for the dual unitary model. It is unclear at present which operators these correspond to. The error bars in c_{eff} and x_i^{typ} only include the uncertainty in the averaged measurement record (estimated via bootstrapping) and α as discussed in the Supplemental Material [37].

In the stabilizer circuit models, we have also extracted the order parameter exponent using an improved numerical method with the results given in Table I. Further details are provided in the Supplemental Material [37], where we also generalize the order parameter exponent to an infinite hierarchy of "purification" exponents with distinct behavior from the minimal-cut percolation model. We further improve our precision in extracting the order parameter exponent by using a dual-unitary Clifford model, where each two-qubit gate is drawn randomly from the uniform set of dual-unitary Clifford gates. The critical $p_c = 0.205(1)$ of this model violates a conjectured bound on $p_c \leq 0.1893$ in $1+1$ dimensions arising from the Hashing bound for the depolarizing channel [13]. In this dual-unitary Clifford model, we observe a significant difference from the percolation value for the order parameter exponent, providing convincing evidence that these models lie in different universality classes.

TABLE I. Critical data for the various models: effective central charge c_{eff}, order-parameter exponent x_1, and whether order-parameter correlations exhibit multifractality (MF). For critical points exhibiting multifractality, we have quoted the order-parameter exponent governing *typical* correlations (marked with †). This is not strictly comparable to the exponent governing *average* correlations quoted for the three other models.

	Haar	Dual unitary	Clifford	Dual Clifford	$d = \infty$ Haar/Clifford
c_{eff}	0.25(3)	0.24(2)	0.37(1)		0.2914/0.3652
x_1	0.14(2)†	0.122(1)†	0.120(5)	0.111(1)	0.1042
MF	✓	✓	✗	✗	✗

Multifractality.—The exponent x_1^{typ} captures how the correlation function of the order parameter, $G_1^{\mathbf{m}}(t)$—defined through $\ln G_1^{\mathbf{m}}(t) = t(\lambda_1^{\mathbf{m}} - \lambda_0^{\mathbf{m}})$—decays as $t \to \infty$ in a *typical* trajectory $\mathbf{m}$. Specifically, $\overline{\ln G_1^{\mathbf{m}}(t)} \sim -(2\pi t/L)x_1^{\text{typ}}$, when $t \gg L$, see Eq. (4), where $\overline{(\ldots)}$ denotes an average over trajectories. Below, we suppress the trajectory index $\mathbf{m}$. Quantities such as $\ln G_1(t)$ are self-averaging and can be extracted numerically. However, the decay of the *sample-averaged* correlation function $\overline{G_1(t)}$ and its moments, $\overline{G_1(t)^n} \sim \exp[-2\pi t x_1(n)/L]$ (in the limit $t \gg L$), are governed by a continuous family of critical exponents $x_1(n)$ due to multifractal scaling at the critical point of the Haar transition. We characterize the multifractal scaling through the distribution function $P[Y(t)]$ where $Y(t) \equiv -\ln G_1(t)$. If this correlation function exhibits multifractal scaling, its distribution will follow the universal scaling form [32]

$$P[Y(t)] \sim \left(\frac{2\pi\alpha t}{L}\right)^{-1/2} \exp\left[-\frac{2\pi\alpha t}{L} H\left(\frac{Y(t)}{2\pi\alpha t/L}\right)\right], \qquad (5)$$

for some (universal) function $H(s)$. As shown in Fig. 2, our numerical results for various system sizes and times, when rescaled according to Eq. (5) collapse onto a single curve, demonstrating multifractality at the Haar critical point. This observation is one of the central results of our work.

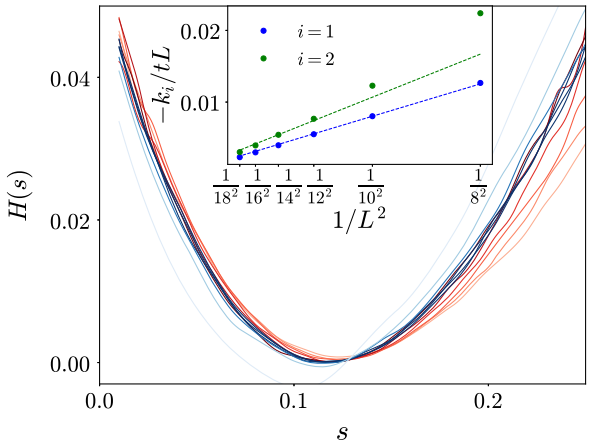

FIG. 2. The scaling collapse of the data onto a universal multifractal scaling function $H(s)$, given by Eq. (5), demonstrates multifractality at the critical point of the Haar transition and corresponds to a continuum of critical exponents. Data are shown for the dual unitary model (a similar quality of collapse also holds for Haar gates [37]) where darker red indicates larger system sizes ($L = 8 \to 18$, $t = 24L$) and darker blue indicates later times ($t = 3L \to 24L$, $L = 16$). (inset) The first two cumulants k_i of $\ln G_1(t)$ divided by tL show the expected $1/L^2$ behavior.

Finally, the exponents $x_1(n)$ are connected to the scaling function $H(s)$; one can use the standard relation between moments and cumulants

$$\ln \overline{G_1(t)^n} = n\overline{\ln G_1(t)} + \frac{n^2}{2!}\overline{(\ln G_1(t) - \overline{\ln G_1(t)})^2} + \ldots, \tag{6}$$

where all terms are self-averaging, to find an expansion for the nth moment exponent $x_1(n) = nx_1^{(1)} + (n^2/2!)x_1^{(2)} + \cdots$, valid at small n. (Here, $x_1^{(1)} = x_1^{\mathrm{typ}}$.) In the inset of Fig. 2, we see that the first two cumulants $k_{1,2}$ of $\ln G_1(t)$ have, when divided by tL, the expected $\sim 1/L^2$ scaling. We estimate $x_1^{(1)} = 0.14(2)$, $x_1^{(2)} = 0.15(2)$ for the Haar model and $x_1^{(1)} = 0.122(1)$, $x_1^{(2)} = 0.145(2)$ for the dual unitary model. The substantial value of $x_1^{(2)}$ indicates that multifractality is strong: the average and typical exponents are appreciably different.

Concluding, we studied the effective central charge and critical exponents for a variety of random circuit models of measurement-induced criticality. We found strong evidence that the transitions in the Haar, Clifford, and percolation problems belong to three distinct universality classes. Using the dual unitary variation of these models, we extracted accurate values for the aforementioned quantities. Additionally, we have clear evidence of multifractal scaling and thus a continuous spectrum of scaling dimensions at the transition in the Haar model.

A. Z. and J. H. P. are partially supported by Grant No. 2018058 from the United States-Israel Binational Science Foundation (BSF), Jerusalem, Israel. J. H. P. acknowledges support from the Alfred P. Sloan Foundation through a Sloan Research Fellowship. A. Z. is partially supported through a Fellowship from the Rutgers Discovery Informatics Institute. J. H. W. acknowledges the Aspen Center for Physics where part of this work was performed, which is supported by National Science Foundation Grant No. PHY-1607611. R. V. acknowledges support from the Air Force Office of Scientific Research under Grant No. FA9550-21-1-0123, and the Alfred P. Sloan Foundation through a Sloan Research Fellowship. S. G. acknowledges support from NSF No. DMR-1653271. The authors acknowledge the Beowulf cluster at the Department of Physics and Astronomy of Rutgers University and the Office of Advanced Research Computing (OARC) at Rutgers, The State University of New Jersey for providing access to the Amarel cluster, and associated research computing resources that have contributed to the results reported here. The Flatiron Institute is a division of the Simons Foundation. D. A. H. is supported in part by the DARPA DRINQS program.

[1] B. Skinner, J. Ruhman, and A. Nahum, Phys. Rev. X **9**, 031009 (2019).
[2] Y. Li, X. Chen, and M. P. A. Fisher, Phys. Rev. B **98**, 205136 (2018).
[3] A. Chan, R. M. Nandkishore, M. Pretko, and G. Smith, Phys. Rev. B **99**, 224307 (2019).
[4] Y. Li, X. Chen, and M. P. A. Fisher, Phys. Rev. B **100**, 134306 (2019).
[5] M. J. Gullans and D. A. Huse, Phys. Rev. X **10**, 041020 (2020).
[6] S. Choi, Y. Bao, X.-L. Qi, and E. Altman, Phys. Rev. Lett. **125**, 030505 (2020).
[7] A. Zabalo, M. J. Gullans, J. H. Wilson, S. Gopalakrishnan, D. A. Huse, and J. H. Pixley, Phys. Rev. B **101**, 060301(R) (2020).
[8] C.-M. Jian, Y.-Z. You, R. Vasseur, and A. W. W. Ludwig, Phys. Rev. B **101**, 104302 (2020).
[9] Y. Bao, S. Choi, and E. Altman, Phys. Rev. B **101**, 104301 (2020).
[10] M. J. Gullans and D. A. Huse, Phys. Rev. Lett. **125**, 070606 (2020).
[11] Y. Li, X. Chen, A. W. W. Ludwig, and M. P. A. Fisher, Phys. Rev. B **104**, 104305 (2021).
[12] M. Szyniszewski, A. Romito, and H. Schomerus, Phys. Rev. Lett. **125**, 210602 (2020).
[13] R. Fan, S. Vijay, A. Vishwanath, and Y.-Z. You, Phys. Rev. B **103**, 174309 (2021).
[14] A. Lavasani, Y. Alavirad, and M. Barkeshli, Nat. Phys. **17**, 342 (2021).
[15] S. Sang and T. H. Hsieh, Phys. Rev. Research **3**, 023200 (2021).
[16] M. Ippoliti, M. J. Gullans, S. Gopalakrishnan, D. A. Huse, and V. Khemani, Phys. Rev. X **11**, 011030 (2021).
[17] Y. Fuji and Y. Ashida, Phys. Rev. B **102**, 054302 (2020).

[18] O. Alberton, M. Buchhold, and S. Diehl, Phys. Rev. Lett. **126**, 170602 (2021).
[19] N. Lang and H. P. Büchler, Phys. Rev. B **102**, 094204 (2020).
[20] X. Chen, Y. Li, M. P. A. Fisher, and A. Lucas, Phys. Rev. Research **2**, 033017 (2020).
[21] O. Lunt and A. Pal, Phys. Rev. Research **2**, 043072 (2020).
[22] A. Nahum and B. Skinner, Phys. Rev. Research **2**, 023288 (2020).
[23] C.-M. Jian, B. Bauer, A. Keselman, and A. W. W. Ludwig, arXiv:2012.04666.
[24] S.-K. Jian, C. Liu, X. Chen, B. Swingle, and P. Zhang, Phys. Rev. Lett. **127**, 140601 (2021).
[25] G. Bentsen, S. Sahu, and B. Swingle, Phys. Rev. B **104**, 094304 (2021).
[26] A. Nahum, S. Roy, B. Skinner, and J. Ruhman, PRX Quantum **2**, 010352 (2021).
[27] S. Gopalakrishnan and M. J. Gullans, Phys. Rev. Lett. **126**, 170503 (2021).
[28] C. Noel, P. Niroula, D. Zhu, A. Risinger, L. Egan, D. Biswas, M. Cetina, A. V. Gorshkov, M. J. Gullans, D. A. Huse, and C. Monroe, arXiv:2106.05881.
[29] J. Napp, R. L. La Placa, A. M. Dalzell, F. G. Brandao, and A. W. Harrow, arXiv:2001.00021.
[30] K. Noh, L. Jiang, and B. Fefferman, Quantum **4**, 318 (2020).
[31] R. Vasseur, A. C. Potter, Y.-Z. You, and A. W. W. Ludwig, Phys. Rev. B **100**, 134203 (2019).
[32] A. W. W. Ludwig, Nucl. Phys. **B330**, 639 (1990).
[33] A. W. W. Ludwig and J. L. Cardy, Nucl. Phys. **B285**, 687 (1987).
[34] *different from* the prefactor of the log of subsystem size in the entanglement entropy which is instead a (boundary) scaling dimension [8,31].
[35] M. Levin and C. P. Nave, Phys. Rev. Lett. **99**, 120601 (2007).
[36] J. L. Jacobsen and J. Cardy, Nucl. Phys. **B515**, 701 (1998).
[37] See Supplemental Material at http://link.aps.org/supplemental/10.1103/PhysRevLett.128.050602 for additional data and details on the numerical method for computing the critical point, free energy density, and estimating the anisotropy parameter in the Haar, dual unitary, and stabilizer circuit models. Purification exponents in stabilizer circuits and minimal-cut percolation models. Exact expressions for the effective central charge for the large onsite Hilbert space dimension limit.
[38] S. Aaronson and D. Gottesman, Phys. Rev. A **70**, 052328 (2004).
[39] B. Bertini, P. Kos, and T. Prosen, Phys. Rev. Lett. **123**, 210601 (2019).
[40] S. Gopalakrishnan and A. Lamacraft, Phys. Rev. B **100**, 064309 (2019).
[41] P. Hayden, S. Nezami, X.-L. Qi, N. Thomas, M. Walter, and Z. Yang, J. High Energy Phys. 11 (2016) 009.
[42] T. Zhou and A. Nahum, Phys. Rev. B **99**, 174205 (2019).
[43] D. Gross, S. Nezami, and M. Walter, Commun. Math. Phys. **385**, 1325 (2021).